REPORT DOCUMENTATION PAGE

Form Approved
OMB No. 0704-0188

1. REPORT DATE *(DD-MM-YYYY)*	2. REPORT TYPE	3. DATES COVERED *(From - To)*
30-Sep-2009	REPRINT	

4. TITLE AND SUBTITLE
IMPROVED PHASE CHARACTERIZATION OF FAR-REGIONAL BODY WAVE ARRIVALS IN CENTRAL ASIA

5a. CONTRACT NUMBER
FA8718-06-C-0002

5b. GRANT NUMBER

5c. PROGRAM ELEMENT NUMBER
62601F

6. AUTHOR(S)
Aaron Ferris, Delaine Reiter, and Katherine Murphy

5d. PROJECT NUMBER
1010

5e. TASK NUMBER
SM

5f. WORK UNIT NUMBER
A1

7. PERFORMING ORGANIZATION NAME(S) AND ADDRESS(ES)

Weston Geophysical Corporation
181 Bedford St., Suite 1
Lexington, MA 02420

8. PERFORMING ORGANIZATION REPORT NUMBER

9. SPONSORING / MONITORING AGENCY NAME(S) AND ADDRESS(ES)
Air Force Research Laboratory
29 Randolph Road
Hanscom AFB, MA 01731-3010

10. SPONSOR/MONITOR'S ACRONYM(S)
AFRL/RVBYE

11. SPONSOR/MONITOR'S REPORT NUMBER(S)
AFRL-RV-HA-TR-2009-1064

12. DISTRIBUTION / AVAILABILITY STATEMENT
Approved for Public Release; Distribution Unlimited.

13. SUPPLEMENTARY NOTES
Reprinted from: Proceedings of the 2009 Monitoring Research Review – Ground-Based Nuclear Explosion Monitoring Technologies, 21 – 23 September 2009, Tucson, AZ, Volume I pp 42 - 51.

14. ABSTRACT

The early body-wave coda of far-regional events (14° – 29° degrees) contains triplicated arrivals from upper-mantle discontinuities that, when properly identified, can improve seismic monitoring functions. However, far-regional seismograms are typically under-utilized because along-path heterogeneity and phase interactions make the arrival suite difficult to interpret accurately. We have developed a set of techniques for small aperture arrays that improve phase characterization and identification at these distances. We have focused our efforts on two arrays in Kazakhstan (MKAR and KKAR), which record far-regional events throughout South-Central Asia. Our techniques include improved array processing methods (e.g., phase-weight semblance stacking) to characterize arrival time, back-azimuth and slowness of individual phases within the *P*-coda arrival suite, and methods to more accurately identify the measured arrivals (e.g., tau-p transformation and clustering analysis to determine wavefield templates).

The most direct means of phase identification is through matching arrival time and slowness estimates to theoretical predictions. In complex tectonic regions such as South-Central Asia, global reference models perform poorly at farregional distances, and more specific knowledge of the along-path and near-array earth structure is required for confident primary and secondary phase identification. To account for near-array effects on the array measurements, we use receiver functions to image below the arrays. Receiver functions allow a direct estimate of the structure below the array (e.g. Moho dip), independent of the array measurements and without bias to other along-path effects. We then use array measurements (slowness and arrival times) to empirically derive regionalized velocity-depth profiles that more accurately predict the far-regional phase succession. These are based on tau-p transformation of both array measurements and waveforms to form generalized representations of the along-path earth structure that is sensitive to far-regional propagation. To understand the far-regional phase behavior not predicted by tau-p ray methods, we use the velocity-depth profiles to synthesize suites of seismograms that are used as part of a waveform clustering algorithm. The clustering algorithm processes array beams to derive 'wavefield templates', i.e., grouped observations with similar phase characteristics. The wavefield templates are further analyzed in a non-linear fashion by comparing them with the synthetic seismograms, looking for quantitative explanations for the phase behaviors not predicted by tau-p ray methods. This work has resulted in a methodology that improves the usefulness of small-aperture array in the phase characterization of far-regional earthquakes. Our research has also yielded insight into body-wave phases that are regularly observed on the MKAR and KKAR arrays, including information on expected wave propagation behavior and the regional nature of the upper-mantle discontinuities.

15. SUBJECT TERMS
Far-regional, Triplications, Wavefield templates

16. SECURITY CLASSIFICATION OF:			17. LIMITATION OF ABSTRACT	18. NUMBER OF PAGES	19a. NAME OF RESPONSIBLE PERSON
a. REPORT	b. ABSTRACT	c. THIS PAGE			Robert J. Raistrick
UNCLAS	UNCLAS	UNCLAS	SAR	10	19b. TELEPHONE NUMBER *(include area code)*

IMPROVED PHASE CHARACTERIZATION OF FAR-REGIONAL BODY WAVE ARRIVALS IN CENTRAL ASIA

Aaron Ferris[1], Delaine Reiter[1], and Katherine Murphy[1]

Weston Geophysical Corporation

Sponsored by the Air Force Research Laboratory

Award No. FA8718-06-C-0002

ABSTRACT

The early body-wave coda of far-regional events (14°– 29° degrees) contains triplicated arrivals from upper-mantle discontinuities that, when properly identified, can improve seismic monitoring functions. However, far-regional seismograms are typically under-utilized because along-path heterogeneity and phase interactions make the arrival suite difficult to interpret accurately. We have developed a set of techniques for small aperture arrays that improve phase characterization and identification at these distances. We have focused our efforts on two arrays in Kazakhstan (MKAR and KKAR), which record far-regional events throughout South-Central Asia. Our techniques include improved array processing methods (e.g., phase-weight semblance stacking) to characterize arrival time, back-azimuth and slowness of individual phases within the *P*-coda arrival suite, and methods to more accurately identify the measured arrivals (e.g., tau-p transformation and clustering analysis to determine wavefield templates).

The most direct means of phase identification is through matching arrival time and slowness estimates to theoretical predictions. In complex tectonic regions such as South-Central Asia, global reference models perform poorly at far-regional distances, and more specific knowledge of the along-path and near-array earth structure is required for confident primary and secondary phase identification. To account for near-array effects on the array measurements, we use receiver functions to image below the arrays. Receiver functions allow a direct estimate of the structure below the array (e.g. Moho dip), independent of the array measurements and without bias to other along-path effects. We then use array measurements (slowness and arrival times) to empirically derive regionalized velocity-depth profiles that more accurately predict the far-regional phase succession. These are based on tau-p transformation of both array measurements and waveforms to form generalized representations of the along-path earth structure that is sensitive to far-regional propagation. To understand the far-regional phase behavior not predicted by tau-p ray methods, we use the velocity-depth profiles to synthesize suites of seismograms that are used as part of a waveform clustering algorithm. The clustering algorithm processes array beams to derive 'wavefield templates', i.e., grouped observations with similar phase characteristics. The wavefield templates are further analyzed in a non-linear fashion by comparing them with the synthetic seismograms, looking for quantitative explanations for the phase behaviors not predicted by tau-p ray methods. This work has resulted in a methodology that improves the usefulness of small-aperture array in the phase characterization of far-regional earthquakes. Our research has also yielded insight into body-wave phases that are regularly observed on the MKAR and KKAR arrays, including information on expected wave propagation behavior and the regional nature of the upper-mantle discontinuities.

OBJECTIVE

The objective of our research is to enhance the usefulness of regional, small-aperture arrays by developing array-based methods that can more accurately characterize far-regional (14°-29°) *P*-coda arrivals. At these distances seismograms are particularly interesting, due to multipathing through the lithosphere and upper-mantle. A suite of body-wave arrivals is often observed in a short time window (1-20 seconds) that bottom near the discontinuities at 220 km, 410 km, and 660 km depth, depending on epicentral distance and along-path structure. The arrivals can be closely spaced in time and exhibit amplitude anomalies related to triplication effects. When these arrivals can be properly identified they can be used to further enhance information regarding seismic source parameters, as well as earth structure. However, far-regional seismograms exhibit significant complexity due to regional heterogeneity and interference effects from depth-phase multiples and near-receiver scattered arrivals. It is the goal of this project to improve the characterization of the far-regional arrivals from South-Central Asian events by employing refined array processing techniques.

The regional seismic arrays that have been built in the last fifteen years should be a rich data source for the study of far-regional phase behavior. The arrays are composed of high-quality borehole seismometers that make high fidelity, low-noise recordings. However, beyond regional distances, the small apertures of these arrays (< 5km) limit their usefulness beyond first-arrival *P*- and S- onset picks. Standard array methods (e.g., slant stacking and frequency-wavenumber analysis) poorly resolve the azimuth and slownesses of primary and secondary arrivals, making confident arrival identification and classification quite difficult. We are overcoming this limitation by applying refined array processing techniques in conjunction with straightforward wavefield generalization methodologies. Our goal is to characterize the commonly observed early coda arrivals that propagate from the different seismic regions of South-Central Asia, utilizing recordings from the Makanchi (MKAR) and Karatau (KKAR) arrays in Kazakhstan (Fig. 1). This research improves the usefulness of small-aperture arrays by increasing their ability to classify small-magnitude events that may be poorly recorded regionally and teleseismically.

RESEARCH ACCOMPLISHED

We have developed array-based methodologies to characterize the *P* coda of far-regional events using small aperture arrays. Our methodology includes several components: 1) enhanced array calibration to account for near-array structure; 2) improved small-aperture array processing to effectively measure delay-times (τ) and slownesses (p) of primary and secondary arrivals; 3) construction of region-specific velocity-depth profiles derived from the τ-p measurements (i.e., τ-p transformations), as well as models derived from wavefield continuation methods; and 4) the derivation of 'wavefield templates' from clustering of array beams to capture the commonly observed arrival structure. These methods employ both theoretical and empirical techniques to reduce a large waveform dataset (~600 earthquakes; Fig. 1) into a smaller set of robustly observed wave phenomena. We then attempt to explain these phenomena using well-accepted, straightforward techniques. The separate components of our methodologies are discussed below.

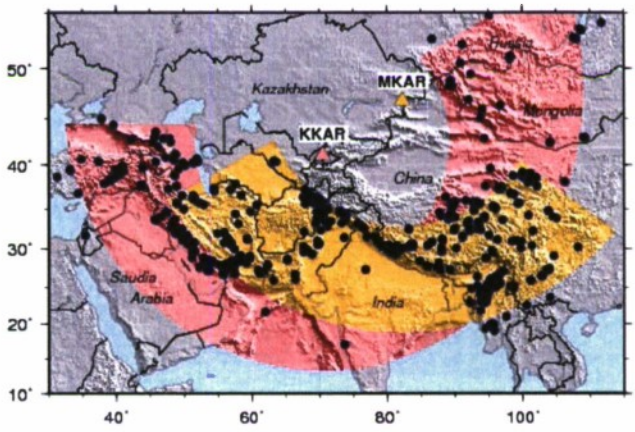

Figure 1. Map of South-Central Asia showing the location of the Makanchi (MKAR) and Karatau (KKAR) arrays in Kazakhstan, as well as earthquakes (circles) used in this study. Colored bands mark the 14°-29° distance range from each array.

Near-Array Earth Structure from Receiver Functions

Array-based observations of slowness and back-azimuth typically deviate from 1D earth predictions because of structural heterogeneity along the ray path. These deviations need to be corrected in order to confidently identify particular arrivals. In many cases, heterogeneities directly below the array can account for most of the observed anomalies (e.g. Niazi, 1966; Havskov and Kansewich, 1978). Interactions with upper mantle structure, such as topographic relief on the discontinuities, can also produce anomalous observations. At the MKAR and KKAR arrays, we observe both back-azimuth and slowness anomalies, where azimuth residuals are ±20° in some instances. We think that near-array structure, as well as along-path effects, contribute to these observations.

A common method to account for near-array structure is to calibrate the array by correcting the array-based measurements to theoretical values of slowness and back-azimuth. For example, published earthquake epicenters are used to determine the expected great-circle azimuth angle, and a 1D earth model is used to compute expected ray parameters. In the case of a single non-lateral interface, (e.g., dipping Moho), the azimuth and slowness residuals, relative to the theoretical values, have a sinusoidal pattern with respect to back-azimuth. The amplitude and phase of these patterns can be used to solve for dip and strike of the interface, and thus a correction can be computed for each event based on its observed back-azimuth angle. This method works well only if near-array structure causes the anomalous residuals, the residuals are systematic with respect to back-azimuth, and there is good azimuth coverage of array measurements. However, for the MKAR and KKAR arrays these criteria are not well met, and we require a different approach.

To obtain a more accurate accounting of the near-array structure, and thus improve our array measurements, we are employing receiver function techniques to image the structure below the arrays. Our goal is to separate near-array effects on the azimuth and slowness measurements from the far-off path effects by accounting for the near-array structure independent of the array measurements. Determining structure from receiver functions has several benefits over array-based methods: 1) only the near-array structure is imaged and far-off path effects have no influence, 2) earth structure is not determined from the measurements you are trying to correct (the array measurements in our case), and 3) teleseismic events used for the receiver functions are more azimuthally distributed compared to the far-regional events.

For the MKAR and KKAR arrays, we compute receiver functions using data from the single 3-component instrument installed at each array using a time domain deconvolution method. The distribution of teleseismic events is shown in Figure 2, displayed as the Moho *P*-to-*S* conversion points around each array. Several hundred receiver functions are computed for each array. The distribution for the MKAR array is more azimuthally complete than the KKAR array, but we are attempting to acquire more events to fill the gaps. Receiver function images are shown in Figure 3 for MKAR and Figure 4 for KKAR.

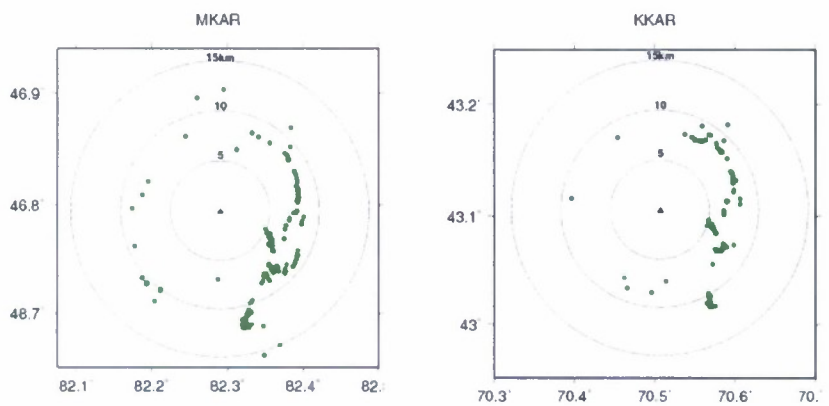

Figure 2. Azimuthal distribution of teleseismic events used in the receiver function calculations. The green dots mark the Moho conversion point for each of the receiver functions.

Using the radial and tangential receiver functions we form azimuthal record sections to image *P*-to-*S* converted phases below each array. The record sections (Figures 3 and 4) are constructed by stacking receiver functions at constant azimuth spacing. To account for variation in ray parameter of the teleseismic events and to minimize incoherent scattered energy, we use a 2D Gaussian weighting function where the weight is a function of nearness to the back-azimuth stacking point and ray parameter (Neal and Pavlis, 1999). In this manner, we are able to construct an evenly sampled (in back-azimuth), smoothed record sections that can be used in subsequent analysis.

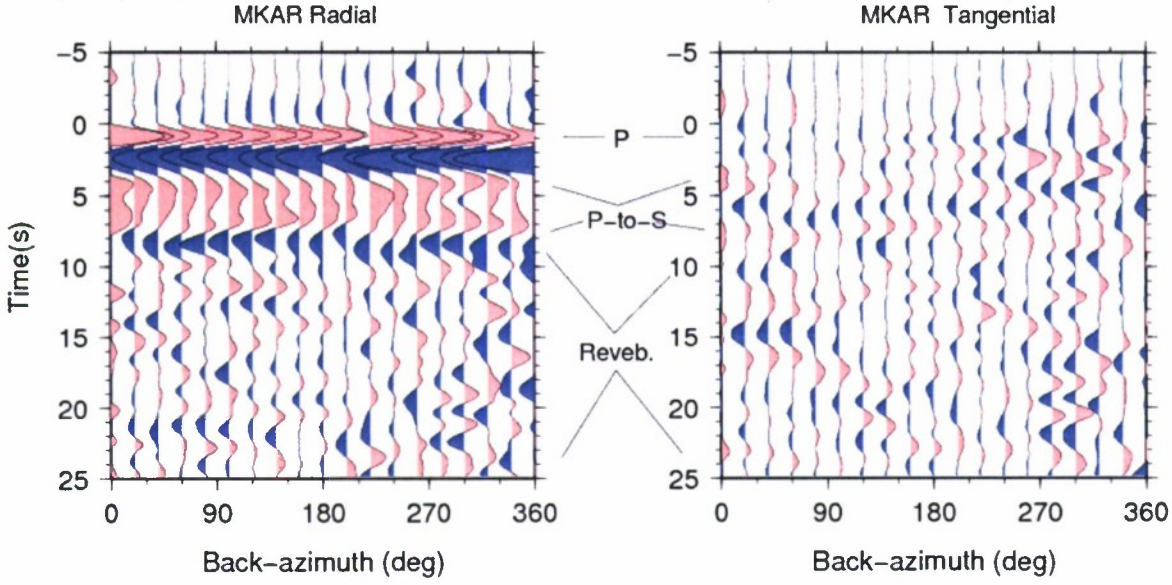

Figure 3. MKAR receiver functions record sections. The receiver functions are aligned on the minimum-phase time and have been filtered at 0.1 to 0.4 Hz.

Figures 3 and 4 show the MKAR and KKAR record sections. The main *P*-to-*S* signal at both MKAR and KKAR has a delay of ~6.0 seconds for the high-frequency band we are examining. It is most obvious in the radial component sections, and it shows some variation in arrival-time and amplitude for different back-azimuths. Preceding this phase is a large amplitude negative pulse, which may be related to a low-velocity zone near the surface. Later arriving reverberations are also apparent in both the MKAR and KKAR sections and show variations with back azimuth. Coherent energy is apparent on the tangential component sections, which is typically indicative of dipping structure or, in some cases, anisotropy. Coherent energy on the tangential components is clearest in KKAR record sections, where amplitude polarity changes are also seen. However, observed phases and the coherency of the record sections seem to have frequency dependence. At lower frequencies, the main *P*-to-*S* phase is less prominent and the tangential record sections are less coherent (not shown). This may be related to the nature of the velocity contrasts across the discontinuities below the arrays, and will likely be sorted out from our analysis

We are still in the process of analyzing and interpreting the receiver function images. The moveout of the radial component reverberations and the existence of coherent energy on the tangential components receiver functions seem to imply that the earth structure below the arrays is not laterally homogeneous, as we expected from the array measurements. In order to understand the earth structure we are taking a simple forward modeling approach. We start with a simple flat-layer velocity model determined from inverting a cumulative stack of the radial receiver functions. Using this model, we systematically vary the strike and dip of the Moho to compute a suite of synthetic receiver functions. The synthetic radial and tangential record sections are then quantitatively compared to the observed record sections. In this manner we are trying to solve for the strike and dip that minimizes the difference between the observed and computed record sections. Preliminary results from this exercise for the MKAR array show that much of the receiver function arrival structure can be explained by a prominent discontinuity at 48 km depth striking 210° N with a dip of 10°.

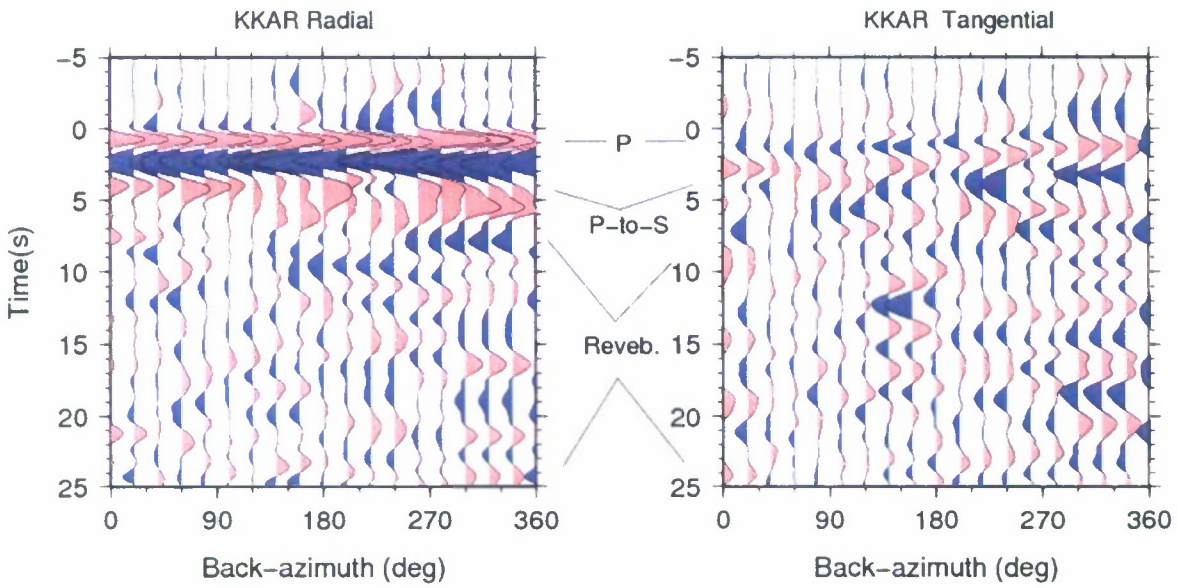

Figure 4. KKAR receiver function record sections. The receiver functions are aligned on the minimum-phase time and have been filtered at 0.1 to 0.4 Hz.

Improved Small-Aperture Array Processing

Our objective for the array processing is to compile a set a phase delay times (τ), back-azimuth and slowness measurements (p) and array beams for our waveform data set of ~600 earthquakes. The small aperture (< 5 km) of many of the newer arrays installed for nuclear monitoring purposes presents a serious challenge for typical array processing methods at far-regional distances. The restricted array aperture and limited number of array channels provides limited resolving power, particularly for slowness measurements. However, we have developed and applied a phase-weight semblance stacking method that improves the usage of small-aperture arrays at far-regional distances. The method combines an amplitude unbiased measure of coherency, the phase-weight stack (e.g. Schimmel and Paulssen, 1997), with semblance, an energy coherency measure. By combining the two coherency measures the signal-to-noise level is increased without detrimentally affecting small amplitude, emergent arrivals. The semblance stack also has the added benefit of being directly related to the F statistic, allowing confidence testing at particular signal-to-noise levels. Our results indicate that in many cases we can detect closely-spaced arrivals by their slowness values in a time window that includes the direct *P* arrival, depth phases and arrivals from upper-mantle discontinuities (Ferris and Reiter, 2007).

In Figure 5 we show two examples of applying the phase-weight semblance stacking to far-regional events recorded by the MKAR array. The first event was recorded at a distance of 25° where the main *P* arrivals bottom near the 660 km discontinuity and appear in the first few seconds of the seismograms. The other dominant phases are the *pP* and *sP* depth phase packets that follow a similar path, exhibiting similar slowness structure as the main P arrivals (as seen in the slowness vespagram) but increased signal amplitude. The second event was recorded at a distance 14.9°. At this distance the first arrivals are *Pn* followed by arrivals bottoming near 220 km depth. Later arrivals include the *P*410 phase (~8 seconds later), followed by larger amplitude *P*410 depth phases.

The back azimuth vespagrams show variations in azimuth over the 20-second arrival window of the *P* phases. This is most evident for the event at 25° distance and reflects out of plane effects from along-path and near-array heterogeneity. While the slowness vespagrams are able to isolate the individual arrivals as a function of time, the phase weight semblance shows smearing in the slowness dimension. This is a related to wave-number aliasing and is a function of the array configuration. Further improvement to the slowness and azimuth vespagrams may only be realized by increasing the number of sensors at the arrays and modifying its geometry.

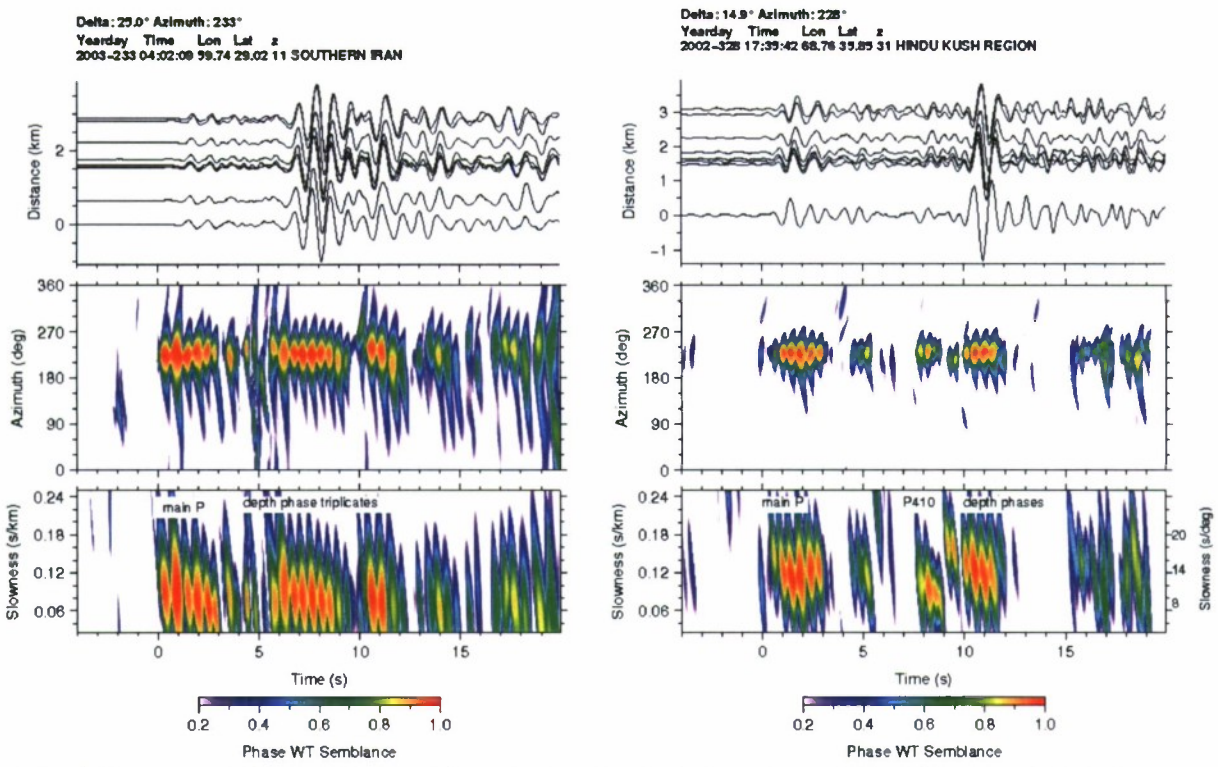

Figure 5. Example of phase-weight semblance processing for two separate earthquakes recorded by the MKAR array at a epicentral distance of 25° (left) and 14.9° (right). The top row shows the array gathers, the middle row shows the arrival back-azimuth vespagrams, and the bottom row shows the slowness vespagrams.

As part of the slowness and back-azimuth measurement exercise we compared our slowness estimates to those predicted by the AK135 reference model. This illuminated the need for more region-specific models in order to make accurate identifications. The next component of our improved phase characterization scheme uses the array measurement and subsequent array beams to derive models that can more accurately match the observations. Our methodologies to accomplish this and results are discussed in the following sections.

Regional Velocity Depth Profiles

To address the need for more applicable earth models and to generalize our array observations, we derived velocity-depth profiles for the specific regions monitored by the MKAR and KKAR arrays. We employed two methods based on τ-p (i.e. delay-time/slowness) techniques that decompose wavefields into their components parts. The first method involves applying wavefield continuation techniques (i.e., τ-p transformations) to the array-based delay-time and slowness measurements to solve for a velocity-depth function through a migration procedure. The second method applies the same techniques to full-waveform record sections, accomplishing the same goal (e.g., McMechan, 1984). While these methods are not new, they are not typically applied to small-aperture array data, but rather to data from long linear arrays of seismometers (e.g., Morozov et al., 2005). Since we apply these methods to multiple events records, a main challenge is accounting for the effects of differing source parameters (origin time, event depth, and focal mechanism), which may be unknown or poorly constrained. Our results show that we are able to extract reasonable models for specific regions in our study area that can more consistently match observed arrival parameters.

Figure 6 illustrates how we prepare array-based delay-time and slowness measurements for velocity-depth inversion. In this example we groom the outliers from data set of measurements made at MKAR, consisting of 110 earthquakes ranging from 14°-29° epicentral distance, which includes earthquakes extending from the Hindu Kush region of Pakistan/Afghanistan to the Makran coast and Zagros Mountains of Iran. The grooming removes everything outside

the 8.0 – 14.5 (sec/deg) slowness range, to help eliminate measurements from *P*-to-*S* scattered signals and coherent noise. We also discard measurements that exhibit significant slowness smearing (i.e., large measurement uncertainties) during the processing. Once the groomed measurements (Figure 6a) have been collected, we reduce them to a single r-*p* curve by computing the error-weighted-mean r value within evenly spaced slowness bins (Figure 6b), excluding bins with only a few measurements. Averaging the r's within a common slowness bin acts to correct for errors in focal depth by accounting for the $\pm\tau$ offset between *P* and *pP*. While this is not a perfect correction due to missed phases in the array processing, the inclusion of *sP* arrivals, and measurement error, we have found it more effective and feasible than correcting τ on an event basis using catalog depths, which typically have large uncertainties. The averaged r-*p* curves, while useful in their own right, are further processed in velocity-depth using wavefield continuation methods, which we describe below as applied to full-waveform record sections.

The wavefield continuation method consists of two linear transformations of the wavefield. These are illustrated in Figure 7. First, record sections are slant stacked, transforming them from the distance-time domain into the r-*p* domain (Figure 7b). This is followed by a downward continuation, or depth migration, of the wavefield to transform the r-*p* data to the slowness-depth plane. This second step is an iterative process, where the τ-*p* data are repeatedly migrated until the slowness-depth image converges to the input velocity model (Figure 7c). There are several ways to update the velocity model between iterations. We are currently using a scheme that picks the maximum amplitude at each depth from the slowness-depth image and then computing the weighted average between it in the input velocity model. This scheme performs adequately; however, noise in the initial τ-*p* transformation can cause artifacts in the final velocity-depth profile that needs to be corrected *a posteriori*.

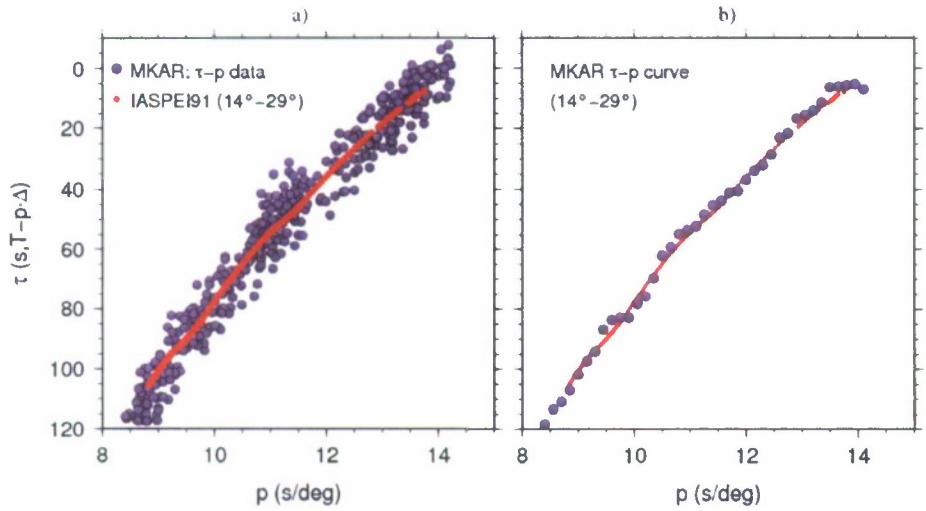

Figure 6. Sample τ-*p* data from the MKAR array. a) The groomed MKAR data (blue circles); red dots show the iasp91 τ-*p* curve for a surface-focus source. The range in τ for a particular slowness is caused by the difference in τ for earthquakes at different depths, rather than just measurement error. b) The averaged τ-*p* curve from the groomed data, evenly sampled in slowness at 0.15 sec/deg.

The resulting velocity-depth profiles show general agreement between the array-based measurement transforms and full-waveform transforms. The models more accurately match the far-regional arrival observations at MKAR and KKAR than reference models such as iasp91 and AK135. The main upper-mantle discontinuities are found at 250 km, 415 km and 670 km depth (Fig 7). In general, the wavefield continuation results exhibit moderately slower velocities than iasp91 below 250 km depth, and a gradient zone is observed near 410 km depth rather than a sharp discontinuity.

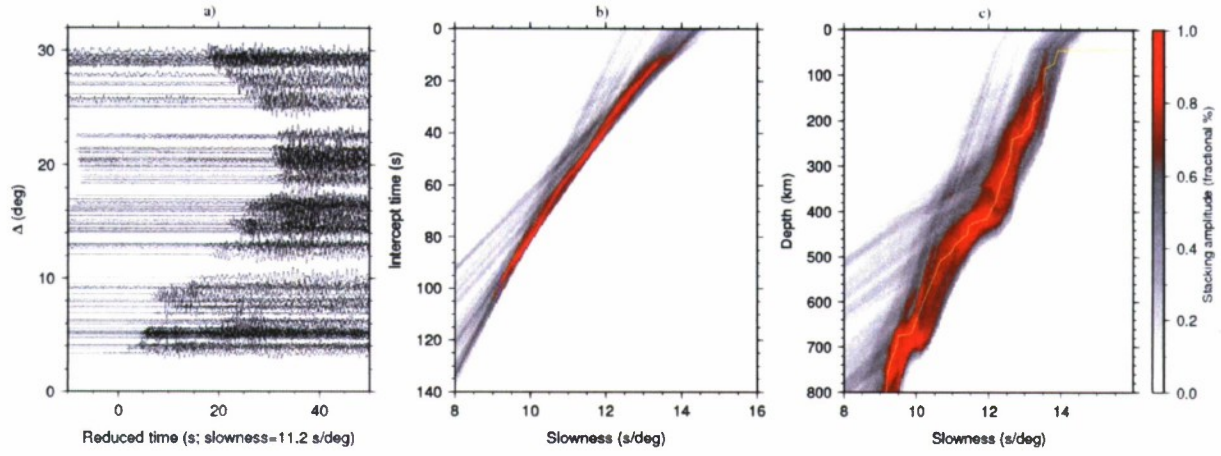

Figure 7. Example showing the transformation of a record section (a) to the τ-p domain (b) and the downward continuation to the slowness-depth domain (c). Array beams are from 104 earthquakes that extend from the Hindu Kush region of Pakistan/Afghanistan to the Makran coast and Zagros mountains of Iran.

Waveform Templating for Groups of Like Waveforms

Another component of our phase characterization methodology is the analysis of the array beams using clustering techniques. In addition to the arrival times and slowness of the coda phase arrivals, phase-weight semblance stacking analysis yields array beams, which are then input to a waveform clustering algorithm. The algorithm is based on 'fuzzy clustering' to form groups of beams that exhibit similar characteristics; it has been used widely in pattern recognition applications (Bezdek, 1981). Clusters are defined by assigning each beam a cluster membership value, which is a quantitative measure that incorporates a distance measure between each array beam and a representation of the cluster centers. We have experimented with distance measures involving *L1* and *L2* norms, as well as waveform semblance, with varying degrees of success that depend on data noise levels. From each cluster of similar beams, we derive a template waveform using a stacking process that weights each cluster member by its degree of membership to that particular cluster. The 'fuzziness' of the method allows a single beam to be a member of more than one cluster group. The objective behind the waveform clustering is to reduce the database of observations to a set of representative waveforms that exhibit consistent phase arrival behavior. Sometimes the clustering is geographic, but there are other wave phenomena that can also produce groupings of similar waveforms

Figure 8a shows the cluster group and its associated wavefield template that results from applying our waveform clustering algorithm to the set of 100 events shown in Figure 8b. These beams are derived from seismograms recorded by the MKAR array in the 14°-29° distance range that extends from northern Pakistan to the Makran coast in Iran. In this example the algorithm clusters the events into 5 groups, with 12-24 members per group. We applied an *L2*-norm distance measure and aligned the array beams prior to clustering using multi-channel cross correlation applied to the first four seconds of each beam signal. We have found the alignment of the beams to be beneficial to the clustering procedure. However, the length of the cross-correlation window is an important variable. For example, if the window is too long, the array beams align on the maximum amplitude signal in the record. For some beams the maximum amplitude arrival may occur early in the seismogram, while for others it occurs much later. This can result in some unusual clustering of events that seems counter-intuitive. For this reason, we find clustering methods based strictly on cross correlation, as used in other types of studies (e.g., Menke 1999) are not suitable for our particular needs.

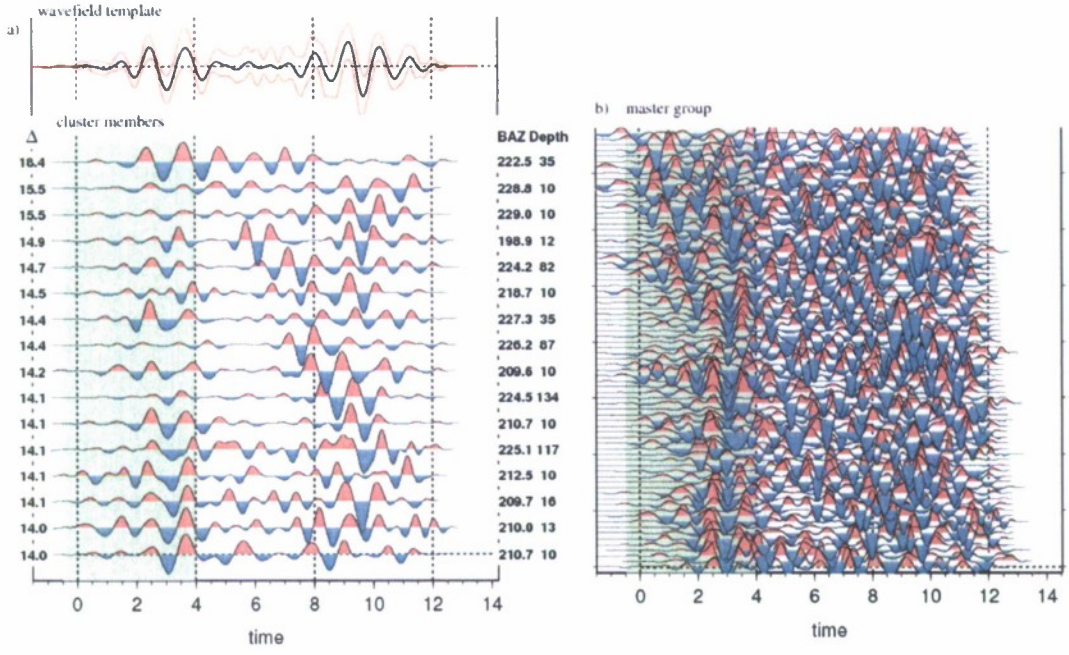

Figure 8. Example of wavefield clustering to generate a wavefield template. (a) The bottom panel shows the cluster members sorted by epicentral distance (shown on the left). The green band highlights the time band of cross correlation. The top panel shows the computed wavefield template (black) and 1-σ deviation (red). (b) A record section of all 100 earthquakes input to the clustering algorithm.

For the example shown in Figure 8, the resulting cluster members include earthquakes that are near the 14.3° distance range, but some more distant earthquakes are also included. The earthquake depth range is also variable, but may be due to poorly constrained catalog depths. In general, the cluster members show consistent waveform structure in the cross-correlated portion of the signal. Later arrivals show more variability between the cluster members, but still appear to align well at approximately 8 seconds and later. The most variability occurs between 4 and 8 seconds delay time, where some records show large amplitude arrivals while other show little signal. Some of this variability is likely due to differences in earthquake distance, triplicated arrivals, and the presence of depth phases. We continue to refine and improve the wavefield clustering algorithm.

Phase Characterization Analysis

A final component of our far-regional methodology is to characterize the observed phase arrivals. One way we have been attempting to do this is to quantitatively compare arrivals predicted from the derived velocity-depth profiles to those observed in the 'wavefield templates'. The purpose of this exercise is to determine how much of the arrival structure can be explained by simple and straightforward methods and models. Using these velocity-depth models we generate a suite of synthetic seismograms, which we then use to compute several different misfit measures between the synthetics and the observed wavefield templates. Since the synthetic waveforms are generated from models derived from the τ-p data, arrival times of the wavefield templates should be well matched. We note that to derive meaningful measurements we must account for frequency content and amplitude variations.

While this exercise in waveform modeling is relatively crude, we are finding general agreement between the synthetic waveforms and the 'wavefield' templates. This suggests to us that a significant portion of the observed far-regional arrival structure can be explained by regional-specific 1D models.

CONCLUSIONS AND RECOMMENDATIONS

Regional seismic arrays that have been recently installed for nuclear monitoring are under-utilized in the study of far-regional arrivals. The small aperture of many of these arrays (< 5km) restricts their usefulness at these distances

beyond first arrival onset picks of *P* and *S* waves. However, our research is overcoming this limitation by applying refined array processing techniques in conjunction with τ-p and wavefield templating analysis methods. Our methodology improves the characterization of primary and early coda phase arrivals observed at far-regional and near-teleseismic distances. Our approach is to distill the wide variety of seismicity we observe to subsets of commonly and robustly observed phase arrival phenomena. We are then using well-accepted modeling and inversion techniques to explain these phenomena. Our aim is to explain as much of the phenomena as we can with simple and straightforward techniques, leaving the anomalies for future research

We are developing and applying our techniques to South-Central Asian earthquakes recorded on the MKAR and KKAR arrays in Kazahkstan. Our results indicate that we can differentiate between the numerous arrivals of the early P-coda. However, global reference models cannot capture the phase succession and arrival-time behavior we observe from the complex tectonic regions of South-Central Asia. To address this, we have developed regional 1D models directly from the array measurements (delay-times, slowness, and beams). Since these models are derived from the data, they are able to explain the phase behavior we observe from specific regions. To test these models and further improve phase characterization, we have constructed 'wavefield templates' through cluster analysis to generalize the waveform structure from the difference seismic regions. The templates are then used in a waveform fitting analysis to gain a better understanding of the phase phenomenon observed from the complex seismic regions of central Asia.

While our methodology improves the usefulness of small-aperture arrays at analyzing far-regional P-coda arrivals, greater gains could be made by installing more elements and increasing the effective array aperture at both MKAR and KKAR. Modifying the array geometry would reduce the wave-number aliasing for arrivals with slowness values between 8-11 s/deg and increasing the aperture would improve both slowness and azimuth resolution. An addition of 2-6 new sensors in an outer-ring configuration would significantly improve far-regional array analysis.

REFERENCES

Bezdek, J. C. (1981). Pattern recognition with fuzzy objective function algorithms, Plenum Press, New York.

Carbonell, R., and S. B. Smithson, (1994). Inversion of reflected *PP*, *SS*, and converted *PS*/*PP* travel times for crustal structure, *Bull. Seism. Soc. Am.* 84: 1889–1902.

Ferris, A. and D. Reiter (2007). Using small-aperture arrays to identify far-regional P-wave arrivals, in *Proceedings of the 29th Monitoring Research Review: Ground-based Nuclear Explosion Monitoring Technologies*, LA-UR-07-5613, Vol. 1, pp. 14–23.

Havskov, J. and E. R. Kanasewich (1978). Determination of the dip and strike of the Moho from array analysis, *Bull. Seism. Soc. Am.* 68: 1415–1419.

McMechan, G. A. (1984). Inversion of a refraction wavefield by imaging in the p-x and v-z planes, *Geophys. J. R. Astr. Soc.* 78: 723–733.

Menke, W. (1999). Using waveform similarity to constrain earthquake location, *Bull. Seism. Soc. Am.* 89: 4, 1141–1146.

Morozov, I. B., E.A. Morozova, S. B. Smithson, P. G. Richards, V. I. Khalturin, and L. N. Solodilov (2005). 3D First-arrival regional calibration model of northern Eurasia, *Bull. Seism. Soc. Am.* 95: 951–964.

Neal, S. L. and G. L. Pavlis (1999). Imaging P-to-S conversions with multichannel receiver functions, *Geophys. Res. Lett.* 26: 2581–2584.

Niazi, M., (1966). Corrections to apparent azimuths and travel-time gradients for a dipping Mohorovocic discontinuity, *Bull. Seism. Soc. Am.* 56: 491–509.

Schimmel N. and H Paulssen, (1997). Noise reduction and detection of weak, coherent signals through phase weighted stacking, *Geophys. J. Int.* 130: 497–505.